The Journal of Physiology

A simulation study on the constancy of cardiac energy metabolites during workload transition

Ryuta Saito[1,2], Ayako Takeuchi[3,4], Yukiko Himeno[5], Nobuya Inagaki[2] and Satoshi Matsuoka[3,4]

[1] *Biology Research Laboratories, Mitsubishi Tanabe Pharma Corporation, Saitama 335-8505, Japan*
[2] *Department of Diabetes, Endocrinology and Nutrition, Graduate School of Medicine, Kyoto University, Kyoto 606-8507, Japan*
[3] *Department of Integrative and Systems Physiology, Faculty of Medical Sciences, University of Fukui, Fukui 910-1193, Japan*
[4] *Department of Physiology and Biophysics, Graduate School of Medicine, Kyoto University, Kyoto 606-8501, Japan*
[5] *Department of Life Science, Ritsumeikan University, Kusatsu, Shiga 525-8577, Japan*

Key points

- The cardiac energy metabolites such as ATP, phosphocreatine, ADP and NADH are kept relatively constant during physiological cardiac workload transition.
- How this is accomplished is not yet clarified, though Ca^{2+} has been suggested to be one of the possible mechanisms.
- We constructed a detailed mathematical model of cardiac mitochondria based on experimental data and studied whether known Ca^{2+}-dependent regulation mechanisms play roles in the metabolite constancy.
- Model simulations revealed that the Ca^{2+}-dependent regulation mechanisms have important roles under the *in vitro* condition of isolated mitochondria where malate and glutamate were mitochondrial substrates, while they have only a minor role and the composition of substrates has marked influence on the metabolite constancy during workload transition under the simulated *in vivo* condition where many substrates exist.
- These results help us understand the regulation mechanisms of cardiac energy metabolism during physiological cardiac workload transition.

Abstract The cardiac energy metabolites such as ATP, phosphocreatine, ADP and NADH are kept relatively constant over a wide range of cardiac workload, though the mechanisms are not yet clarified. One possible regulator of mitochondrial metabolism is Ca^{2+}, because it activates several mitochondrial enzymes and transporters. Here we constructed a mathematical model of cardiac mitochondria, including oxidative phosphorylation, substrate metabolism and ion/substrate transporters, based on experimental data, and studied whether the Ca^{2+}-dependent activation mechanisms play roles in metabolite constancy. Under the *in vitro* condition of isolated mitochondria, where malate and glutamate were used as mitochondrial substrates, the model well reproduced the Ca^{2+} and inorganic phosphate (P_i) dependences of oxygen consumption, NADH level and mitochondrial membrane potential. The Ca^{2+}-dependent activations of the aspartate/glutamate carrier and the F_1F_o-ATPase, and the P_i-dependent activation of Complex III were key factors in reproducing the experimental data. When the mitochondrial model was implemented in a simple cardiac cell model, simulation of workload transition revealed that cytoplasmic Ca^{2+} concentration ($[Ca^{2+}]_{cyt}$) within the physiological range markedly increased NADH level. However, the addition of pyruvate or citrate attenuated the Ca^{2+} dependence of NADH during the workload transition. Under the simulated *in vivo* condition where malate, glutamate,

R. Saito and A. Takeuchi have contributed equally to this work.

 DOI: 10.1113/JP272598

pyruvate, citrate and 2-oxoglutarate were used as mitochondrial substrates, the energy metabolites were more stable during the workload transition and NADH level was almost insensitive to $[Ca^{2+}]_{cyt}$. It was revealed that mitochondrial substrates have a significant influence on metabolite constancy during cardiac workload transition, and Ca^{2+} has only a minor role under physiological conditions.

(Received 9 April 2016; accepted after revision 3 August 2016; first published online 17 August 2016)
Corresponding author S. Matsuoka: Department of Integrative and Systems Physiology, Faculty of Medical Sciences, University of Fukui, 23-3 Matsuokashimoaizuki, Eiheiji-cho, Yoshida-gun, Fukui 910-1193, Japan. Email: smatsuok@u-fukui.ac.jp

Abbreviations ACO, aconitase; AGC, aspartate/glutamate carrier; AGC A_{Ca}, Ca^{2+}-activation term of AGC; ALT, alanine aminotransferase; AST, aspartate aminotransferase; $[Ca^{2+}]_{cyt}$, cytoplasmic Ca^{2+} concentration; $[Ca^{2+}]_{mit}$, mitochondrial Ca^{2+} concentration; C3 A_{Pi}, P_i-activation term of Complex III; CaUni, Ca^{2+} uniporter; C_m, electrical capacitance of mitochondrial inner membrane; DCT, dicarboxylate transporter; $\Delta\Psi$, mitochondrial membrane potential; ICDH, isocitrate dehydrogenase; k_{ATPuse}, coefficient of ATP usage; KHE, K^+/H^+ exchanger; KUni, K^+ uniporter; MCT, monocarboxylate transporter; MDH, malate dehydrogenase; $m\dot{V}_{O_2}$, oxygen consumption; NCX, mitochondrial Na^+/Ca^{2+} exchanger; NHE, mitochondrial Na^+/H^+ exchanger; OGC, 2-oxoglutarate/malate carrier; OGDH, 2-oxoglutarate dehydrogenase; PC, pyruvate carboxylase; PCr, phosphocreatine; PDHC, pyruvate dehydrogenase; P_i, inorganic phosphate; P_iC, phosphate carrier; $[P_i]_{cyt}$, cytoplasmic P_i concentration; $[P_i]_{mit}$, mitochondrial P_i concentration; SCS, succinyl-CoA synthase; SN, F_1F_o-ATPase; SN A_{Ca}, Ca^{2+}-activation term of SN; TCT, tricarboxylate transporter.

Introduction

The heart is a continuously working pump that is energetically driven by hydrolysis of ATP. In the heart, mitochondrial oxidative phosphorylation is the major source of ATP, and ATP is consumed mainly by ATPases such as the Na^+/K^+-ATPase, the sarcoplasmic reticulum Ca^{2+}-ATPase and the myosin-ATPase (Katz, 2010). Since the amount of ATP in the heart is small (~0.7 g in the human heart; Ingwall, 2002), ATP synthesis by mitochondrial oxidative phosphorylation must increase so as to adapt to a rise in cardiac ATP demand. This adaptation was well demonstrated by a rapid increase in cardiac oxygen consumption ($m\dot{V}_{O_2}$) during workload augmentation (Hata *et al.* 1994), resulting in a linear relationship between $m\dot{V}_{O_2}$ and workload (Khouri *et al.* 1965; Hata *et al.* 1994). During a change in the heart's physiological workload, energy metabolites such as ATP, phosphocreatine (PCr), ADP and NADH are maintained at almost constant levels (Balaban *et al.* 1986; Katz *et al.* 1989; Balaban, 2009*a*). Mechanisms underlying the constancy of energy metabolites have been extensively studied. However, the details have not yet been clarified.

Chance and Williams were the first to propose feedback control by ADP (Chance & Williams, 1956), which has been recognized as the fundamental mechanism controlling energy homeostasis (Saks *et al.* 2012). Recently Beard and his colleagues suggested, based on analyses of mathematical mitochondrial model and literature experimental data, that P_i is the primary feedback signal stimulating mitochondrial oxidative phosphorylation *in vivo* (Beard, 2006; Wu *et al.* 2008, 2009). The increase of P_i at high cardiac workload was reported by several studies (Bache *et al.* 1999; Gong *et al.* 2003) although Katz *et al.* (1989) could not detect the P_i increase.

ADP and P_i, which are products of ATP hydrolysis, enter mitochondria and become substrates for ATP synthesis by the mitochondrial F_1F_o-ATPase (SN). Rapid transfer of ATP and ADP between mitochondria and extra-mitochondrial ATP-consuming systems is mediated by phosphotransfer pathways, e.g. creatine kinase, adenylate kinase and glycolysis (Andrienko *et al.* 2003; Saks *et al.* 2012). However, feedback control may not be sufficient to maintain the metabolite constancy. Korzeniewski and his colleagues demonstrated in theoretical studies that the feedback control by ADP and P_i induced large changes in energy metabolites during a physiological workload change (Korzeniewski *et al.* 2005; Korzeniewski, 2007). They demonstrated that metabolite constancy can be achieved only by a direct activation of all oxidative phosphorylation complexes and substrate dehydrogenation in parallel with an increase in ATP usage (parallel activation). Zhou *et al.* supported the parallel activation hypothesis, using a more detailed mitochondrial model including metabolic pathways and NADH generation (Zhou *et al.* 2006). However, molecular mechanisms underlying parallel activation have not been experimentally clarified so far.

It has been suggested for years that Ca^{2+} plays roles in the regulation of mitochondrial ATP generation (Balaban, 2009*b*; Glancy & Balaban, 2012). Ca^{2+} directly activates

mitochondrial dehydrogenases: pyruvate dehydrogenase (PDHC), isocitrate dehydrogenase (ICDH), and 2-oxoglutarate dehydrogenase (OGDH) (McCormack *et al.* 1990). The importance of the Ca^{2+}-dependent activation of mitochondrial dehydrogenases was also demonstrated by several mathematical models including ours (Cortassa *et al.* 2006; Jo *et al.* 2006), in which transient changes of mitochondrial NADH were successfully reproduced by assuming Ca^{2+}-dependent activation of mitochondrial dehydrogenases. Several studies have suggested that SN is activated by Ca^{2+} (Harris, 1993; Territo *et al.* 2000, 2001), although the mechanism is not yet clear. The aspartate/glutamate carrier (AGC), which consists of a malate–aspartate shuttle together with a 2-oxoglutarate/malate carrier (OGC), has a Ca^{2+}-binding domain facing the cytoplasm and is activated by cytoplasmic Ca^{2+} concentration ($[Ca^{2+}]_{cyt}$) (Murphy *et al.* 1979; Pardo *et al.* 2006; Satrustegui *et al.* 2007).

It is, however, uncertain whether these Ca^{2+}-dependent activation mechanisms, which were revealed mainly in *in vitro* conditions, e.g. isolated mitochondria, contribute significantly to the constancy of energy metabolites during an *in vivo* workload change. Indeed, in mice lacking mitochondrial Ca^{2+} influx via the mitochondrial Ca^{2+} transporter (CaUni encoded by *MCU*), cardiac function was unaffected (Holmstrom *et al.* 2015) or almost normal except for acute cardiac responses following catecholamine stimulation (Kwong *et al.* 2015; Wu *et al.* 2015). The stability of energy metabolites during workload change was not investigated in these studies. In addition, an increase of cardiac workload is not always accompanied by an increase in $[Ca^{2+}]_{cyt}$. Stretching cardiac muscle increases cardiac contraction, a phenomenon known as the Frank–Starling law of the heart. The stretching, however, does not immediately augment Ca^{2+} transients (Allen & Kurihara, 1982; Shimizu *et al.* 2002). Furthermore, allosteric activation by P_i of OGDH (Rodriguez-Zavala *et al.* 2000) and Complex III of the respiratory chain (Bose *et al.* 2003) was proposed as a possible mechanism to maintain metabolite constancy (Beard, 2006; Wu *et al.* 2008).

In this study, we investigated, by utilizing mathematical modelling and simulation, whether the *in vitro* experimental Ca^{2+}- and P_i-activation mechanisms sufficiently account for metabolite constancy during *in vivo* cardiac workload change. Under the experimental condition of isolated mitochondria using malate and glutamate as substrates, the Ca^{2+}-dependent activation of AGC and SN and the P_i-dependent activation of Complex III were found to be key factors. However, under a simulated *in vivo* condition, where other mitochondrial substrates were included, the energy metabolites were more stable and NADH level was almost insensitive to $[Ca^{2+}]_{cyt}$. Results revealed that mitochondrial substrates greatly influence NADH level during cardiac workload transition, and Ca^{2+} has only a minor role in maintaining metabolite constancy under physiological *in vivo* conditions.

Methods

Computational method

We constructed a mathematical model of cardiac mitochondria, using a Java-based simulation platform, simBio (Sarai *et al.* 2006). The ordinary differential equations were integrated with the fourth order Runge–Kutta method. The time step was adaptively changed in a range from 10^{-6} to 10^{-1} ms to shorten the calculation time. The equations and parameters of enzymes and transporters were determined by fitting to data from isolated heart mitochondria as far as possible. The source code (S1) of Java classes and XML files (S1–4) are available as Supporting Information.

Construction of a cardiac mitochondrial model

The mitochondrial model consisted of oxidative phosphorylation, the citric acid cycle, the pyruvate pathway, substrate transporters and ion transporters (Fig. 1). Simulation analyses were performed in the *in vitro* condition of isolated mitochondria, namely without the components shown inside the dotted box in Fig. 1, or in the *in vivo* cardiomyocyte condition with the components shown inside the dotted box in Fig. 1. The model structure was essentially similar to previously published models (Korzeniewski *et al.* 2005; Cortassa *et al.* 2006; Jo *et al.* 2006; Nguyen *et al.* 2007; Wu *et al.* 2007; Dzbek & Korzeniewski, 2008; Wu *et al.* 2008; Bazil *et al.* 2010; Wei *et al.* 2011). The main feature of our model was that major mitochondrial ion/substrate transporters and all the possible Ca^{2+}- and P_i-dependent mechanisms were formulated so as to simulate mitochondrial ion dynamics, substrate metabolism and ATP production. Details are described in Supporting Information, Appendix and Figs S1–S17. The process of β-oxidation of fatty acids was omitted in this model because the experiments referred to in this study were carried out without fatty acids.

The oxidative phosphorylation model was adapted from the model of Dzbek & Korzeniewski (2008). The dependences of Complex I on NADH and ubiquinone, and of Complex III on reduced ubiquinone and cytochrome c were newly added to fit the model to experimental time courses reported by Bose *et al.* (2003) (Fig. S14). Similarly, the dependence of Complex III on P_i was added according to the experiment by Bose *et al.* (2003).

Kinetic models of enzymes in the citric acid cycle were formulated based on experimental data and

previous models (see Supporting Information, Appendix and Figs S1–S8 and S10 for details). Consequently, the process of substrate dehydrogenation used by Dzbek & Korzeniewski (2008) was replaced with a newly formed detailed model of the citric acid cycle. The pyruvate pathways, which consisted of PDHC, pyruvate carboxylase (PC), and alanine aminotransferase (ALT), and the substrate transporters such as the monocarboxylate transporter (MCT), the dicarboxylate transporter (DCT), the tricarboxylate transporter (TCT), OGC and AGC were formulated. Validation of each elemental model is demonstrated in Figs S11–S13.

Mitochondrial ions (Ca^{2+}, Na^+ and K^+) change dynamically and are important for mitochondrial function (Bernardi, 1999; Takeuchi *et al.* 2015). Mitochondrial ion dynamics were reconstructed by incorporating models of CaUni (Nguyen *et al.* 2007), the Na^+/Ca^{2+} exchanger (NCX) (Kim & Matsuoka, 2008), the Na^+/H^+ exchanger (NHE) (Nguyen *et al.* 2007), the K^+ uniporter (KUni) (Dzbek & Korzeniewski, 2008) and the K^+/H^+ exchanger (KHE) (Dzbek & Korzeniewski, 2008). The CaUni model well reproduced the $[Ca^{2+}]_{cyt}$ dependences of CaUni (Kirichok *et al.* 2004). The NCX model, which assumed a $3Na^+/1Ca^{2+}$ exchange, well reproduced our experimental data on the cytoplasmic Na^+ and $[Ca^{2+}]_{cyt}$ dependences of NCX (Kim & Matsuoka, 2008). In addition, the time course of mitochondrial Ca^{2+} concentration ($[Ca^{2+}]_{mit}$) decline upon activation of NCX was comparable to the experimental data (Kim & Matsuoka, 2008) (Fig. S15*A*). Consequently, the steady state relationship between $[Ca^{2+}]_{cyt}$ and $[Ca^{2+}]_{mit}$ (Wan *et al.* 1989) was well reproduced (Fig. S15*B*).

Mitochondrial membrane potential ($\Delta\Psi$) is determined mainly by the electron transfer system

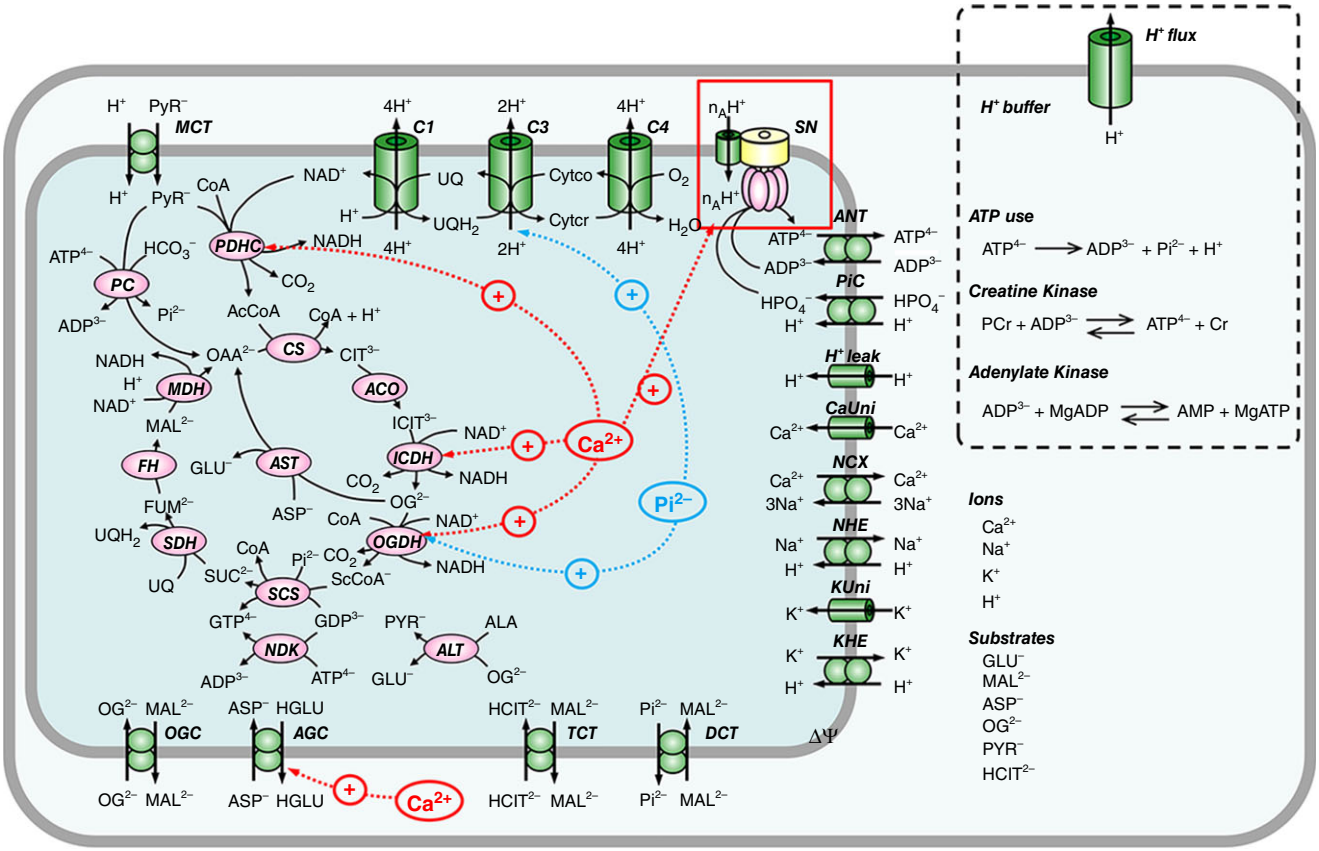

Figure 1. A scheme of the mitochondrial model
Allosteric regulation by Ca^{2+} and P_i is indicated by red and blue arrows, respectively. Shown inside the dotted box are additional cytoplasmic and plasmalemmal components to simulate an *in vivo* workload change of cardiomyocytes with mitochondria incorporated. AcCoA, acetyl-CoA; ALA, alanine; ANT, adenine nucleotide translocase; ASP^-, aspartate; C1, Complex I of the respiratory chain; C3, Complex III of the respiratory chain; C4, Complex IV of the respiratory chain; CS, citrate synthase; Cytco, oxidized form of cytochrome c; Cytcr, reduced form of cytochrome c; FH, fumarate hydratase; FUM^{2-}, fumarate; GLU^-, glutamate; $HCIT^{2-}$, citrate; MAL^{2-}, malate; NDK, nucleoside diphosphate kinase; OAA^{2-}, oxaloacetate; OG^{2-}, 2-oxoglutarate; PYR^-, pyruvate; SDH, succinate dehydrogenase; SUC^{2-}, succinate; UQH2; ubiquinol; ScCoA, succinyl-CoA.

(Complex I, III and IV) and by other electrogenic channels and transporters. Here $\Delta\Psi$ was calculated as follows:

$$\frac{d\Psi}{dt} = -\frac{(4v_{C1} + 2v_{C3} + 4v_{C4} - n_A v_{SN} - v_{LK} - v_{ANT} + v_{AGC} - v_{KUni} - 2v_{CaUni} - v_{NCX})}{C_m}$$

where, C_m is electrical capacitance of mitochondrial inner membrane (0.001 mM mV^{-1}) (Dzbek & Korzeniewski, 2008).

The activation of PDHC, ICDH and OGDH by $[Ca^{2+}]_{mit}$ (McCormack *et al.* 1990) was well reconstructed, as shown in Fig. S16*A–D*. It has been reported that Ca^{2+} activates SN (Harris, 1993; Territo *et al.* 2000; Territo *et al.* 2001), although the mechanisms are not yet clarified. We hypothesized that SN is activated by $[Ca^{2+}]_{mit}$, based on the experimental finding by Territo *et al.* that entry of Ca^{2+} into mitochondria was necessary for SN activation (Territo *et al.* 2000) (Fig. S16*E*). AGC has a Ca^{2+} binding domain facing the extra-mitochondrial space and therefore is activated by $[Ca^{2+}]_{cyt}$ (Murphy *et al.* 1979; Pardo *et al.* 2006; Satrustegui *et al.* 2007). However, since the precise $[Ca^{2+}]_{cyt}$ dependence of AGC was not available, the $[Ca^{2+}]_{cyt}$-dependent activation was expressed as a simple Hill equation in this study (Fig. S16*F*). The parameters of Ca^{2+}-dependent activation of SN and AGC were determined by fitting the models to experimental data (Territo *et al.* 2000; Bose *et al.* 2003).

The activation by mitochondrial P_i concentration ($[P_i]_{mit}$) of OGDH (Rodriguez-Zavala *et al.* 2000) and of Complex III (Bose *et al.* 2003) was determined by fitting the models to experimental data (Fig. S17*A* and *C*). The $[P_i]_{mit}$ dependence of succinyl-CoA synthase (SCS) was reconstructed to reproduce experimental data (Cha & Parks, 1964), as shown in Fig. S17*B*.

Simulation procedures

To simulate *in vitro* experiments on the $[Ca^{2+}]_{cyt}$ dependence of isolated mitochondria performed by Territo *et al.* (Figs 2*A* and 4) (Territo *et al.* 2000), $[Ca^{2+}]_{cyt}$ was changed from 10^{-6} μM to various values (10^{-6}–2.0 μM) for 1 h in the presence of 5 mM malate and 5 mM glutamate as substrates. To simulate *in vitro* experiments on the cytoplasmic P_i concentration ($[P_i]_{cyt}$) dependence of isolated mitochondria performed by Bose *et al.* (Figs 2*B* and 5) (Bose *et al.* 2003), $[P_i]_{cyt}$ was increased from 10^{-6} mM to

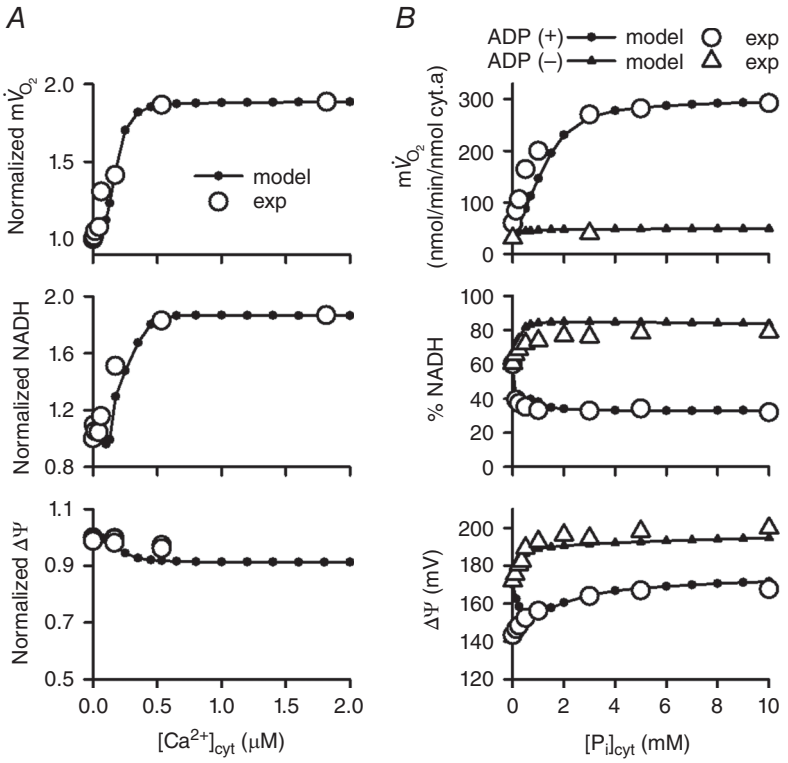

Figure 2. Dependences of $m\dot{V}_{O_2}$, NADH and $\Delta\Psi$ on $[Ca^{2+}]_{cyt}$ and $[P_i]_{cyt}$
Simulations were performed using the model of isolated mitochondria with the experimental conditions of Territo *et al.* (2000) (*A*) and Bose *et al.* (2003) (*B*). *A*, $[Ca^{2+}]_{cyt}$ dependence. Experimental data (exp; open circles) are from Territo *et al.* (2000). Simulation data (model; filled circles) were normalized to those at 10^{-6} μM $[Ca^{2+}]_{cyt}$. *B*, $[P_i]_{cyt}$ dependence. Simulation data (model) were in state III (with ADP, filled circles) and state IV (without ADP, filled triangles). Experimental data (exp; open circles and triangles) were from Bose *et al.* (2003).

various values (10^{-6}–10 mM) for 10 min in the presence of malate/glutamate as substrates. For both simulation procedures, cytoplasmic reactions (shown inside the dotted box in Fig. 1) were omitted. Other initial conditions are listed in Appendix (Supporting Information).

Simulations of cardiomyocytes *in vivo* (Figs 6–11) were performed by incorporating the cardiac mitochondrial model into a simple cardiac cell model (Fig. 1 including the components inside the dotted box) according to the method of Korzeniewski *et al.* (2005). This simple cardiac cell model included cytoplasmic ATP use, creatine kinase, adenylate kinase, cytoplasmic H^+ buffer and H^+ efflux from the cytosol to the extracellular space, in addition to mitochondria. In the model, mitochondrial H^+ leak was reduced to 1% to adjust $m\dot{V}_{O_2}$ level without cardiac workload (Gobel *et al.* 1978; Katz *et al.* 1989; Korzeniewski, 2007). For simulation of *in vitro* experiments with isolated mitochondria (Bose *et al.* 2003), a larger mitochondrial H^+ leak was required to reproduce a mitochondrial pH of 7.14. In the simulations using the simple cardiac cell model, $[Ca^{2+}]_{cyt}$ was changed from 10^{-3} to 10 μM, and the coefficient of ATP usage (k_{ATPuse}) was changed from 1.5×10^{-5} to 1.88×10^{-4} mM ms^{-1} to cover the range of $m\dot{V}_{O_2}$ in dog heart: about 2–11 mM min^{-1} (Boerth *et al.* 1969; Katz *et al.* 1989; Korzeniewski *et al.* 2005). Other initial conditions for each simulation are listed in Appendix (Supporting Information).

Results

Roles of allosteric Ca^{2+}- and P_i-dependent activation

First, we simulated *in vitro* experiments with isolated mitochondria to examine the basic characteristics of the model (Fig. 2). Steady state dependences of $m\dot{V}_{O_2}$, NADH and $\Delta\Psi$ on $[Ca^{2+}]_{cyt}$ and $[P_i]_{cyt}$ were well fitted to experimental data from isolated mitochondria (Territo *et al.* 2000; Bose *et al.* 2003). To study how an individual component contributes to $m\dot{V}_{O_2}$, NADH and $\Delta\Psi$, sensitivity analysis was performed (Fig. 3). As expected, components of oxidative phosphorylation had a great influence on mitochondrial function. The components relating to Ca^{2+}-dependent activation, SN and AGC were influential. In addition, the phosphate carrier (P_iC) and the allosteric P_i-dependent activation of Complex III were also influential. The analysis suggested that Ca^{2+} and P_i have essential roles in mitochondrial function.

Then the contributions of Ca^{2+}- and P_i-dependent activation on $[Ca^{2+}]_{cyt}$ dependence were studied by eliminating individual allosteric regulation by Ca^{2+} or P_i in the simulation of Territo's experimental protocol (Territo *et al.* 2000). In Fig. 4*A*, $[Ca^{2+}]_{cyt}$ dependences of $m\dot{V}_{O_2}$, NADH and $\Delta\Psi$ without Ca^{2+}-dependent activation of AGC (AGC A_{Ca}) or SN (SN A_{Ca}), and without the P_i-dependent activation of Complex III (C3 A_{Pi}), are presented. The ratios of changes in the above parameters when $[Ca^{2+}]_{cyt}$ was increased from 10^{-6} to 0.535 μM are summarized in Fig. 4*B*. The removal of AGC A_{Ca}, SN A_{Ca}, and C3 A_{Pi} had marked effects on the $[Ca^{2+}]_{cyt}$ dependences. Since malate/glutamate were used as mitochondrial substrates, similarly to Territo's protocol (Territo *et al.* 2000), OGC and AGC functioned to supply malate and glutamate to mitochondria (the malate-aspartate shuttle). That is, OGC-mediated malate influx stimulated malate dehydrogenase (MDH) to produce NADH and oxaloacetate. Oxaloacetate was then converted by aspartate amino transferase (AST) to aspartate, leaving mitochondria through AGC. Therefore, AGC functioned to maintain the driving force of OGC to transport malate into mitochondria. The elimination of AGC A_{Ca} therefore reduced $[Ca^{2+}]_{cyt}$-dependent malate supply through the malate-aspartate shuttle, resulting in the reduction of MDH activity to produce NADH. As a result, NADH was depleted, $m\dot{V}_{O_2}$ decreased, and $\Delta\Psi$ depolarized as $[Ca^{2+}]_{cyt}$ increased. The elimination of SN A_{Ca} almost abolished the $[Ca^{2+}]_{cyt}$-dependent increase of $m\dot{V}_{O_2}$ and augmented the $[Ca^{2+}]_{cyt}$-dependent increase of

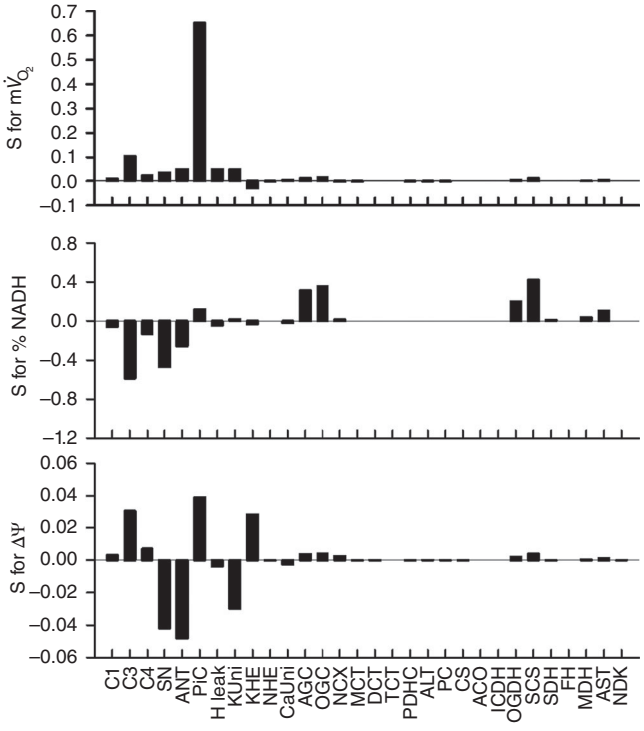

Figure 3. Sensitivity analysis of the isolated mitochondrial model
The simulation conditions were the same as those of Fig. 2*A*, with $[Ca^{2+}]_{cyt} = 1.0$ μM. Sensitivity (S) for parameter X ($X = m\dot{V}_{O_2}$, NADH and $\Delta\Psi$) was calculated as the relative change by ±5% change of the expression level of each component: $S = \frac{|X_{+5\%} - X_{-5\%}|}{0.1 X_{original}}$.

NADH. These alternations were due to the attenuation of function of the respiratory chain. The decline of $\Delta\Psi$ was reversed, or the mitochondrial membrane was hyperpolarized, due to a lower H^+ influx through SN. The elimination of C3 A_{Pi} attenuated the $[Ca^{2+}]_{cyt}$-dependent increase of $m\dot{V}_{O_2}$ and increased NADH because of the attenuation of respiratory chain function. These analyses indicated that the Ca^{2+}-dependent activation of AGC and SN, and the P_i-dependent activation of Complex III are important factors for the $[Ca^{2+}]_{cyt}$ dependences of isolated mitochondrial function.

Similar analyses were performed in Bose's protocol (0.5 μM $[Ca^{2+}]_{cyt}$) with various $[P_i]_{cyt}$ (Bose *et al.* 2003) (Fig. 5). These analyses also demonstrated that the Ca^{2+}-dependent activation of AGC and SN, and the P_i-dependent activation of Complex III are important for the $[P_i]_{cyt}$ dependences of isolated mitochondria.

Metabolite stability and cardiac workload

In order to study the workload dependence of energy metabolites, we used the simple cardiac cell model (Fig. 6). Workload was altered by changing k_{ATPuse} to cover the physiological range of $m\dot{V}_{O_2}$ in dog heart: about 2–11 mM min^{-1} (Boerth *et al.* 1969; Katz *et al.* 1989; Korzeniewski *et al.* 2005). Then simulation was performed at various $[Ca^{2+}]_{cyt}$, from 0.001 to 10 μM. At higher workload, i.e. at higher $m\dot{V}_{O_2}$, cytoplasmic ATP was depleted when $[Ca^{2+}]_{cyt}$ was lower than 0.1 μM, while it was kept constant when $[Ca^{2+}]_{cyt}$ was 0.1 μM or higher. The workload dependences of other metabolites (PCr, ADP, P_i and mitochondrial NADH) at $[Ca^{2+}]_{cyt}$ between 0.1 and 2.0 μM are plotted in Fig. 6*B*. As workload was augmented, ADP and P_i increased, inducing feedback stimulation. The larger increase in P_i than ADP is consistent with previous simulation studies (Beard, 2006; Wu *et al.* 2008; Wu *et al.* 2009). NADH, as well as P_i, was $[Ca^{2+}]_{cyt}$ dependent, suggesting an important role of Ca^{2+}-dependent activation systems for NADH and P_i levels. The $[Ca^{2+}]_{cyt}$ dependence of NADH was mainly due to Ca^{2+}-dependent activation of AGC, as demonstrated in Fig. 4.

It should be noted that the model simulations were performed in the presence of malate/glutamate as mitochondrial substrates, according to the experiments by Bose *et al.* (2003) and Territo *et al.* (2000). Under this condition, the activities of Ca^{2+}-dependent dehydrogenases (PDHC, ICDH and OGDH) were low, as demonstrated later in Fig. 8. It was conceivably possible that NADH was more or differently dependent on $[Ca^{2+}]_{cyt}$ if these dehydrogenases were more active. To test this hypothesis, we studied the dependences of energy metabolites on workload and $[Ca^{2+}]_{cyt}$ at different substrate conditions.

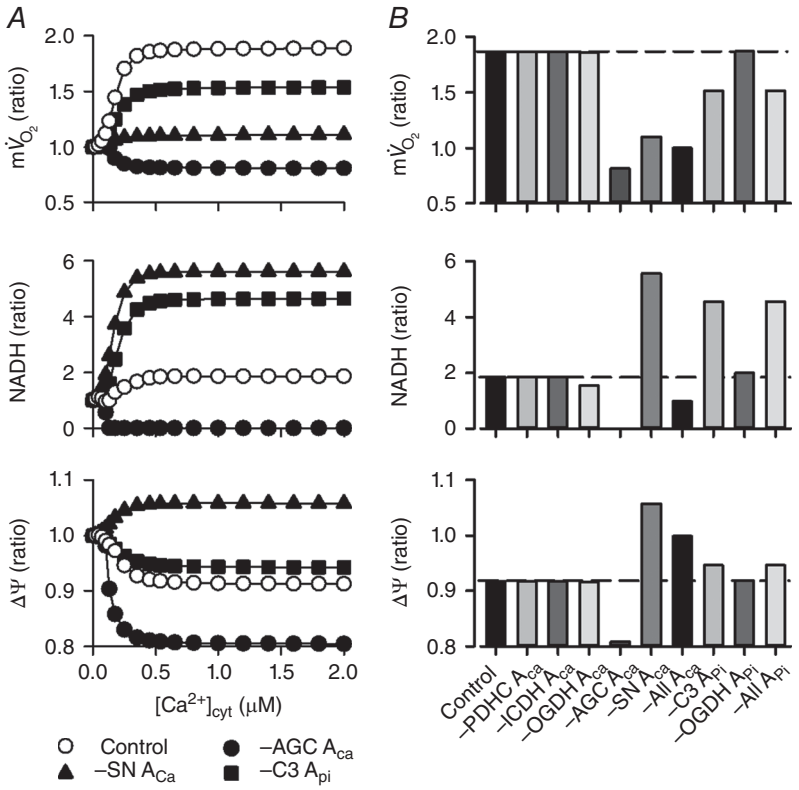

Figure 4. Contribution of the Ca^{2+}- and P_i-dependent activation mechanisms to the $[Ca^{2+}]_{cyt}$ dependences in the isolated mitochondrial model
The basic simulation condition was the same as that of Fig. 2*A*. The Ca^{2+}-dependent activation terms of PDHC, ICDH, OGDH, AGC and SN, that is, PDHC A_{Ca}, ICDH A_{Ca}, OGDH A_{Ca}, AGC A_{Ca} and SN A_{Ca}, were removed from the mathematical formula individually or at the same time. In addition, the P_i-dependent activation terms of Complex III and OGDH, that is, C3 A_{Pi} and OGDH A_{Pi}, were removed individually or at the same time. *A*, removal of AGC A_{Ca}, SN A_{Ca} and C3 A_{Pi}. Open circles represent the control model, and filled symbols represent the absence of AGC A_{Ca}, SN A_{Ca} and C3 A_{Pi}. *B*, summary of the simulation results. Ratios of $m\dot{V}_{O_2}$, NADH and $\Delta\Psi$ at 10^{-6} μM $[Ca^{2+}]_{cyt}$ to those at 0.535 μM $[Ca^{2+}]_{cyt}$ were plotted. Dotted lines indicate the ratios obtained from the control model. –All A_{Ca}: Ca^{2+}-dependent activation terms were removed from all components; –All A_{Pi}: P_i-dependent activation terms were removed from all components.

Substrate dependences of metabolite stability

Pyruvate was added at various concentrations between 0.01 and 10 mM to the cytoplasm, to activate PDHC (Figs 7*A* and 8*B*). When pyruvate concentration was lower than 0.5 mM, mitochondrial NADH increased with increasing $[Ca^{2+}]_{cyt}$ but was almost independent of $[Ca^{2+}]_{cyt}$ at pyruvate concentrations higher than 1 mM (Fig. 7*A*, left panel). This is because higher concentrations of pyruvate stimulated PDHC, overcoming the lower activity of PDHC at low Ca^{2+} concentrations. At a $[Ca^{2+}]_{cyt}$ level in the diastolic heart (0.1 μM; Fig. 7*A*, middle panel), NADH markedly decreased with higher workload when pyruvate concentration was low, while at the mean $[Ca^{2+}]_{cyt}$ level (0.3 μM; Fig. 7*A*, right panel), NADH became relatively stable during workload transition, even at lower pyruvate concentrations. In the physiological range of pyruvate (rat heart: 0.039–0.26 mM) (Albe *et al.* 1990; Kato *et al.* 2010), higher pyruvate concentrations increased NADH level and attenuated the Ca^{2+} dependence of NADH, suggesting the importance of glycolytic flux for NADH stability.

The addition of citrate had a similar tendency to the addition of pyruvate (Fig. 7*B*). Citrate stimulated aconitase (ACO) and ICDH, inducing NADH production by ICDH (Fig. 8*C*). In the physiological range of citrate (0.07–0.39 mM) (Albe *et al.* 1990) and at the mean $[Ca^{2+}]_{cyt}$ level of 0.3 μM, NADH was stable during the workload transition (Fig. 7*B*, right panel).

The addition of 2-oxoglutarate decreased NADH level at all $[Ca^{2+}]_{cyt}$ levels (Fig. 7*C*), although it stimulated NADH production by OGDH (Fig. 8*D*). At physiological concentrations of 2-oxoglutarate (0.07–0.14 mM) (Albe *et al.* 1990), NADH level was dependent on $[Ca^{2+}]_{cyt}$ and was relatively stable during the workload transition at 0.3 μM $[Ca^{2+}]_{cyt}$ (Fig. 7*C*, right panel). An addition of aspartate also markedly decreased mitochondrial NADH (Fig. 7*D*), because high aspartate inhibited conversion by AST from glutamate to aspartate.

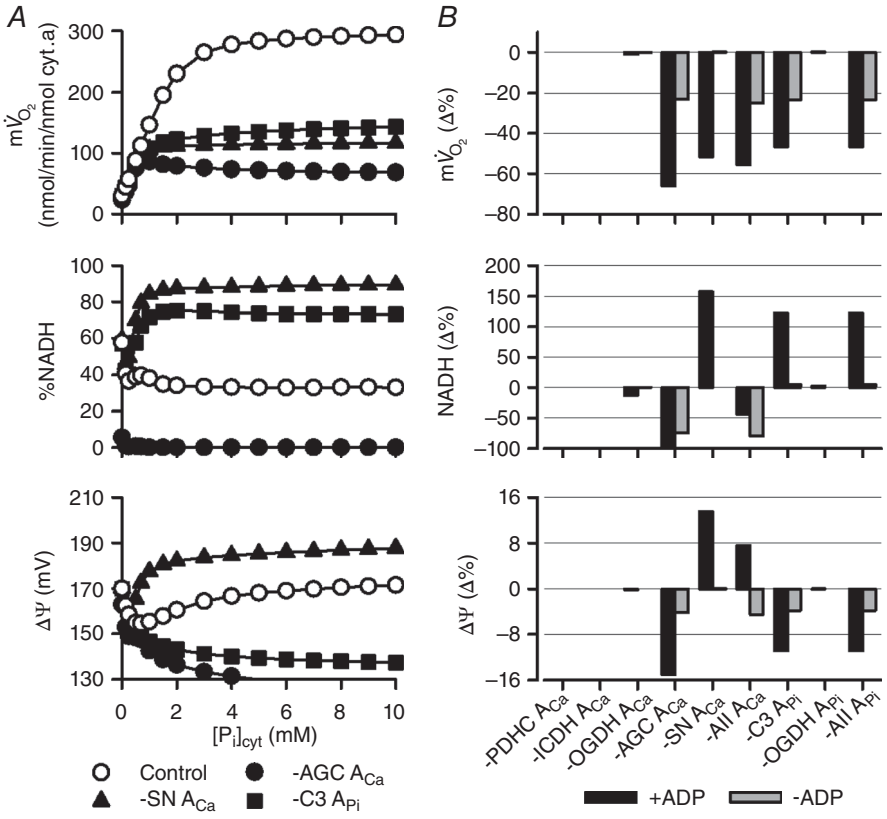

Figure 5. Contribution of the Ca^{2+}- and P_i-dependent activation mechanisms to the $[P_i]_{cyt}$ dependences in the isolated mitochondrial model
The basic simulation conditions were the same as those of Fig. 2*B*. Removal of the Ca^{2+}-dependent activation term and P_i-dependent activation term was the same as in Fig 4. *A*, removal of AGC A_{Ca}, SN A_{Ca} and C3 A_{Pi} under the condition of state III (with $[P_i]_{cyt}$ and ADP in addition to malate/glutamate). Open circles represent the control model, and filled symbols represent the absence of AGC A_{Ca}, SN A_{Ca} and C3 A_{Pi}. *B*, summary. Values of $mV̇_{O_2}$, NADH and $\Delta\Psi$ at 2 mM $[P_i]_{cyt}$ were expressed as percentage difference from the control model. Data are from state III (black) and state IV (with only $[P_i]_{cyt}$ in addition to malate/glutamate; grey).

The above analyses indicated that mitochondrial substrates significantly affect the $[Ca^{2+}]_{cyt}$ dependence of NADH level and the NADH stability during workload transition.

To investigate the stability of mitochondrial NADH under physiological conditions, simulation analysis was performed in the presence of all six substrates at physiological concentrations (Fig. 9): 1 mM malate, 5 mM glutamate, 0.3 mM pyruvate, 0.3 mM citrate, 0.1 mM 2-oxoglutarate and 3 mM aspartate (Albe *et al.* 1990; Kato *et al.* 2010). Under this condition, all of the enzymes of the citric acid cycle and PDHC were active (Fig. 8*F*). Similarly to the malate/glutamate condition (Fig. 6), cytoplasmic ATP could not be maintained at high cardiac workload when $[Ca^{2+}]_{cyt}$ was less than 0.1 μM. Changes of PCr, ADP and P_i were also similar to those under the malate/glutamate condition. However, contrary to the malate/glutamate condition, mitochondrial NADH was almost independent of $[Ca^{2+}]_{cyt}$ and was almost stable during workload change (Fig. 9*B*). $[Ca^{2+}]_{cyt}$ dependence of four dehydrogenases, AGC and OGC were compared between the malate/glutamate condition and this condition in Fig. 10. Under the malate/glutamate condition, the *absence* of cytoplasmic 2-oxoglutarate and aspartate favoured cytoplasmic malate–mitochondrial 2-oxoglutarate exchange via OGC and cytoplasmic glutamate–mitochondrial aspartate exchange via AGC, respectively. Therefore the fluxes through OGC and AGC are large (Fig. 10*A*). The increase of $[Ca^{2+}]_{cyt}$ from 0.1 to 2 μM stimulated AGC resulting in augmentation of NADH production by MDH (the malate–aspartate shuttle). Under the full substrates condition, the *presence* of cytoplasmic 2-oxoglutarate *attenuated* the cytoplasmic malate–mitochondrial 2-oxoglutarate exchange via OGC due to a decreased driving force for outward transport of 2-oxoglutarate. The *presence* of aspartate also *attenuated* the cytoplasmic glutamate–mitochondrial aspartate exchange via AGC due to decreased driving force for outward transport of aspartate (see the equations of OGC and AGC in Supporting Information, Appendix). Therefore, the fluxes through OGC and AGC were smaller than those under the malate/glutamate condition. NADH production by four dehydrogenases was almost independent of $[Ca^{2+}]_{cyt}$ because of very low activity of AGC, lower Ca^{2+} affinity of ICDH (Fig. S15*A*), and the relatively small Ca^{2+}-sensitive component of PDHC (Fig. S16*B*). Under the full substrates condition, pyruvate and malate had significant influence on NADH level, as shown in Fig. 11, where concentration of one substrate was changed at each analysis. Under this condition, the augmentation of mitochondrial influxes of ADP and P_i by their cytoplasmic increases has a pivotal role in the metabolite constancy. Therefore, the metabolite constancy could not be maintained when the augmentation of ANT by increased ADP_{cyt} (Fig. S18*A* and *B*) or the augmentation of P_iC by increased $[P_i]_{cyt}$ (Fig. S18*C*

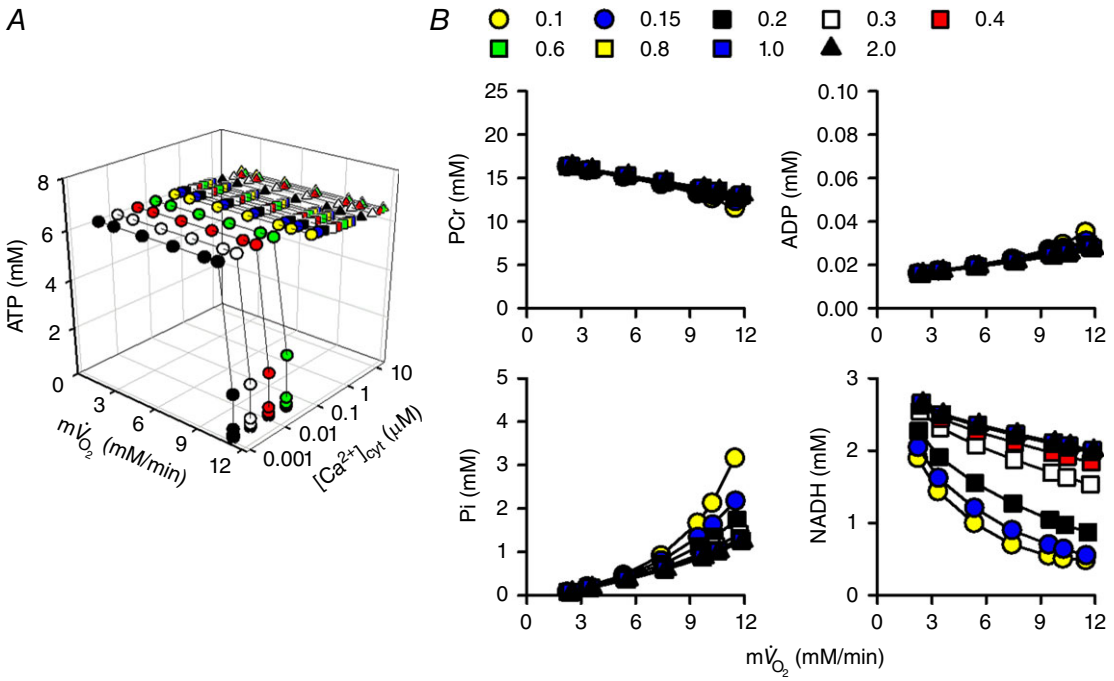

Figure 6. Workload and $[Ca^{2+}]_{cyt}$ dependences of energy metabolites in the simple cardiac cell model
The coefficient of ATP usage, k_{ATPuse}, was changed from 1.5×10^{-5} to 1.88×10^{-4} mM ms^{-1}, and $[Ca^{2+}]_{cyt}$ was changed from 0.001 to 10 μM. *A*, total cytoplasmic ATP. *B*, cytoplasmic PCr, ADP and P_i, and mitochondrial NADH. Data at 0.1 to 2.0 μM $[Ca^{2+}]_{cyt}$ are shown.

and *D*) was eliminated. Allosteric P_i regulation of OGDH and Complex III made a moderate contribution to the metabolite constancy (Fig. S18*E* and *F*).

Discussion

We constructed a mathematical model of cardiac mitochondria including oxidative phosphorylation, substrate metabolism, and ion/substrate transporters, and studied whether the Ca^{2+}-dependent activation mechanisms play roles in metabolite constancy during workload change. The Ca^{2+}-dependent activation mechanisms were prominent at $[Ca^{2+}]_{cyt}$ concentrations below physiological minimum level ($[Ca^{2+}]_{cyt}$ at diastole; approximately 0.1 μM) in cardiomyocytes. When malate and glutamate were sole mitochondrial substrates, as in many experiments using isolated mitochondria, the Ca^{2+}-dependent activation of AGC and SN, and the P_i-dependent activation of Complex III were found to be key factors, and mitochondrial NADH level was

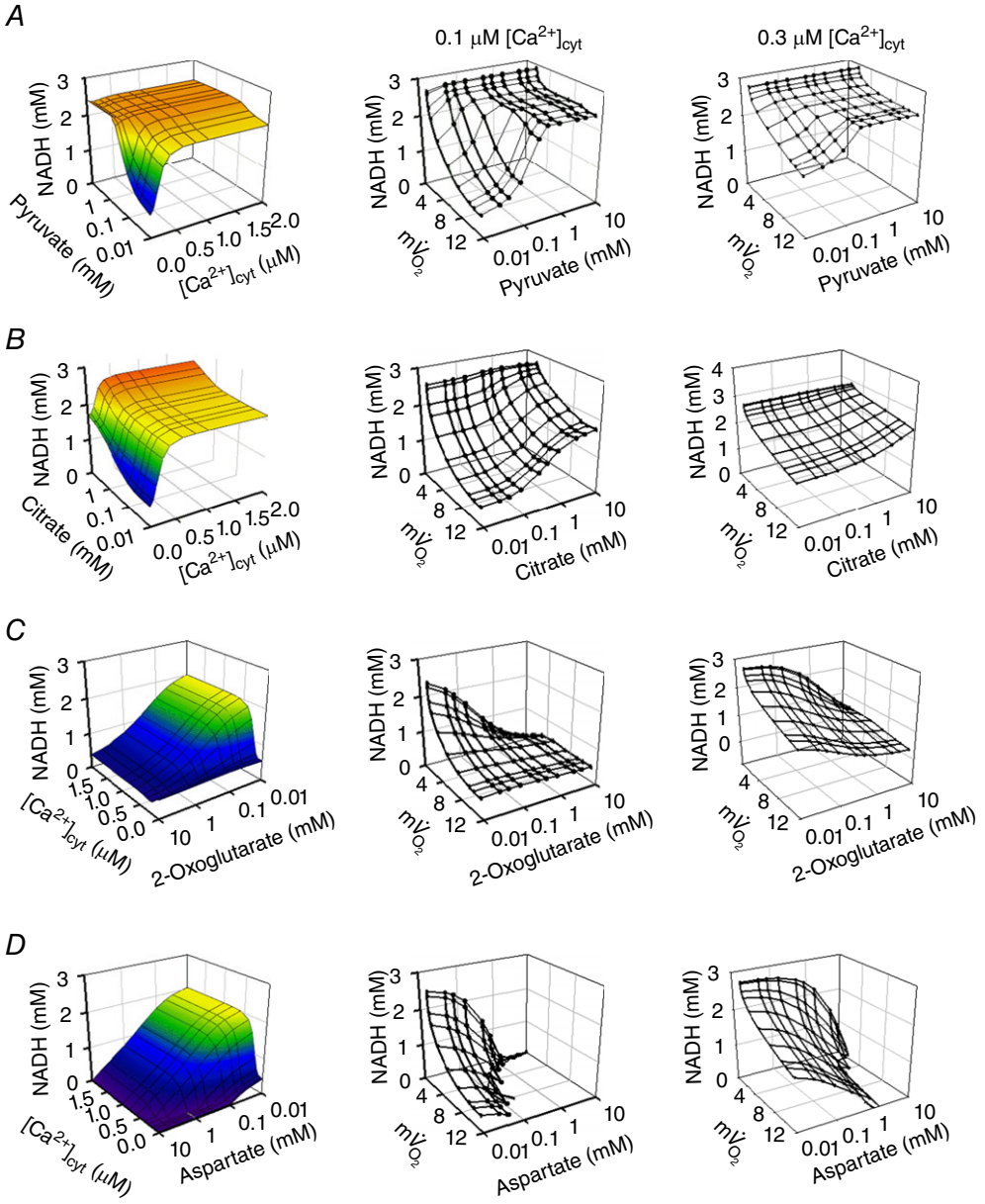

Figure 7. Effects of additional substrate on the workload and $[Ca^{2+}]_{cyt}$ dependences of NADH in the simple cardiac cell model
Pyruvate (*A*), citrate (*B*), 2-oxoglutarate (*C*) and aspartate (*D*) were added to the cytoplasm of the simple cardiac cell model, in addition to malate/glutamate. The middle and right panels show the results of simulations at 0.1 and 0.3 μM $[Ca^{2+}]_{cyt}$, respectively. Unit for $m\dot{V}_{O_2}$ is mM min^{-1}.

increased by $[Ca^{2+}]_{cyt}$ in the physiological range. However, under simulated physiological levels of $[Ca^{2+}]_{cyt}$ and mitochondrial substrates, mitochondrial NADH was relatively constant over the physiological workload change and almost insensitive to $[Ca^{2+}]_{cyt}$. Therefore, it was revealed that mitochondrial substrates greatly influence the NADH level during cardiac workload transition, and Ca^{2+} has only a minor role in maintaining metabolite constancy under physiological conditions.

It has been suggested for years that Ca^{2+} plays roles in the regulation of mitochondrial ATP generation (Balaban, 2009*a*; Glancy & Balaban, 2012). Indeed, implementation

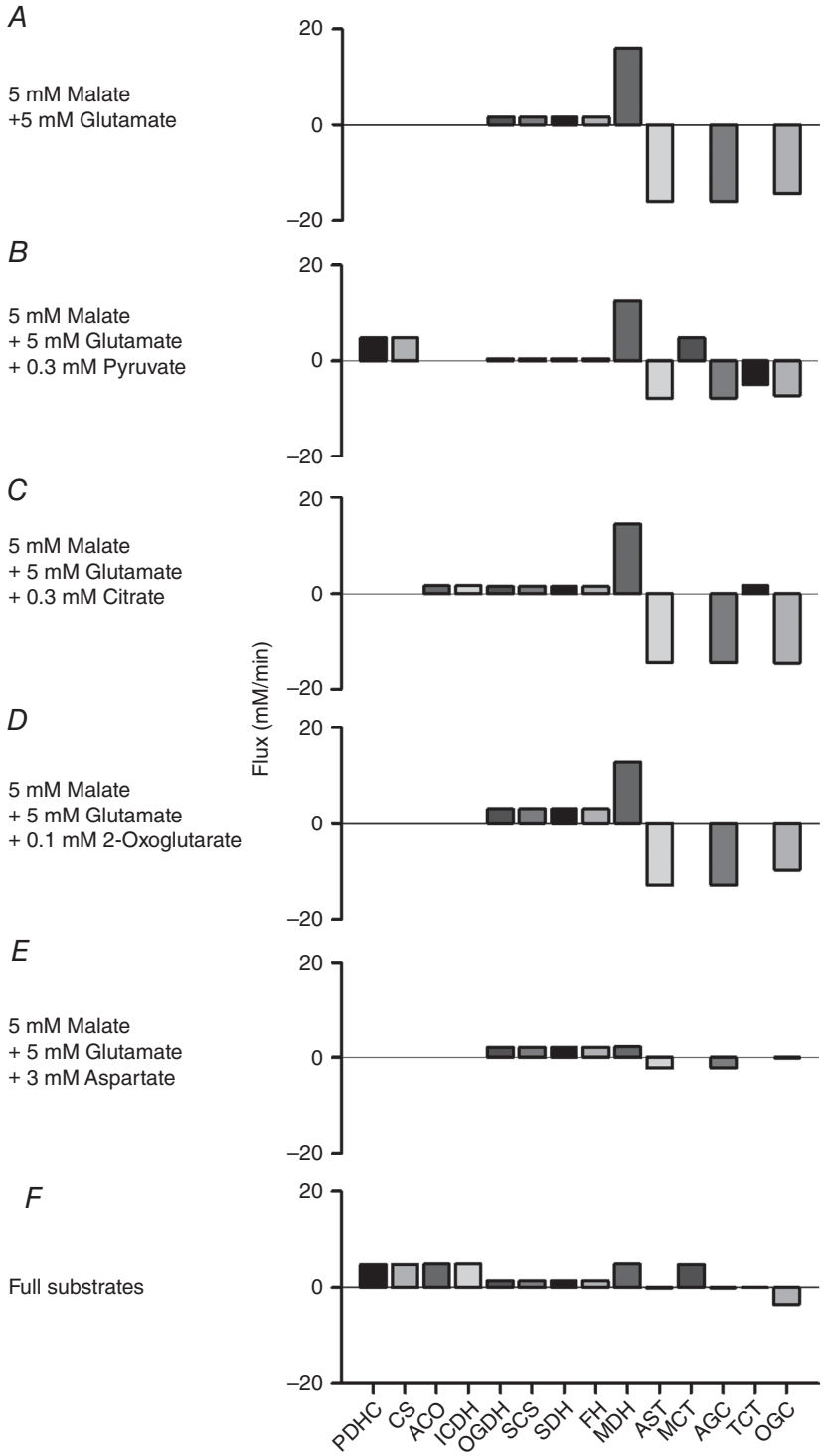

Figure 8. Activities of representative enzymes and substrate transporters at different combinations of substrates in the simple cardiac cell model
A, 5 mM malate and 5 mM glutamate. *B*, 5 mM malate, 5 mM glutamate and 0.3 mM pyruvate. *C*, 5 mM malate, 5 mM glutamate and 0.3 mM citrate. *D*, 5 mM malate, 5 mM glutamate and 0.1 mM 2-oxoglutarate. *E*, 5 mM malate, 5 mM glutamate and 3 mM aspartate. *F*, full substrates; 1 mM malate, 5 mM glutamate, 0.3 mM pyruvate, 0.3 mM citrate, 0.1 mM 2-oxoglutarate and 3 mM aspartate. All the simulations were done at 0.3 μM $[Ca^{2+}]_{cyt}$ and 1.5×10^{-4} mM ms^{-1} k_{ATPuse} ($m\dot{V}_{O_2} = 8.8$ mM min^{-1} except for *E*, 3.2 mM min^{-1}).

of Ca^{2+}-activated systems was inevitable to reproduce experimental data using isolated mitochondria under the malate/glutamate condition (Figs 4 and 5). In addition, Ca^{2+} had pivotal roles in the transient change of NADH upon rapid workload transition, as demonstrated in cardiomyocytes, trabeculae and model simulations (Brandes & Bers, 2002; Cortassa *et al.* 2006; Jo *et al.* 2006). However, under the *in vivo* physiological ranges of $[Ca^{2+}]_{cyt}$ and mitochondrial substrates, the Ca^{2+}-activated systems do not seem to contribute significantly to the steady-state metabolite constancy during workload transition (Fig. 9). At higher workload and lower $[Ca^{2+}]_{cyt}$ below diastolic level (approximately 0.1 μM), energy balance collapsed, suggesting that the basal activation of SN and AGC by Ca^{2+} had significant influences on metabolite constancy. However, since the heart is continuously beating, and $[Ca^{2+}]_{cyt}$ hardly ever decreases below 0.1 μM, the enzymes and transporters could be constitutively activated by Ca^{2+} under physiological conditions. Additionally, the allosteric effects of Ca^{2+} were nearly saturated at the mean $[Ca^{2+}]_{cyt}$ level of cardiomyocytes and could not be expected to have marked

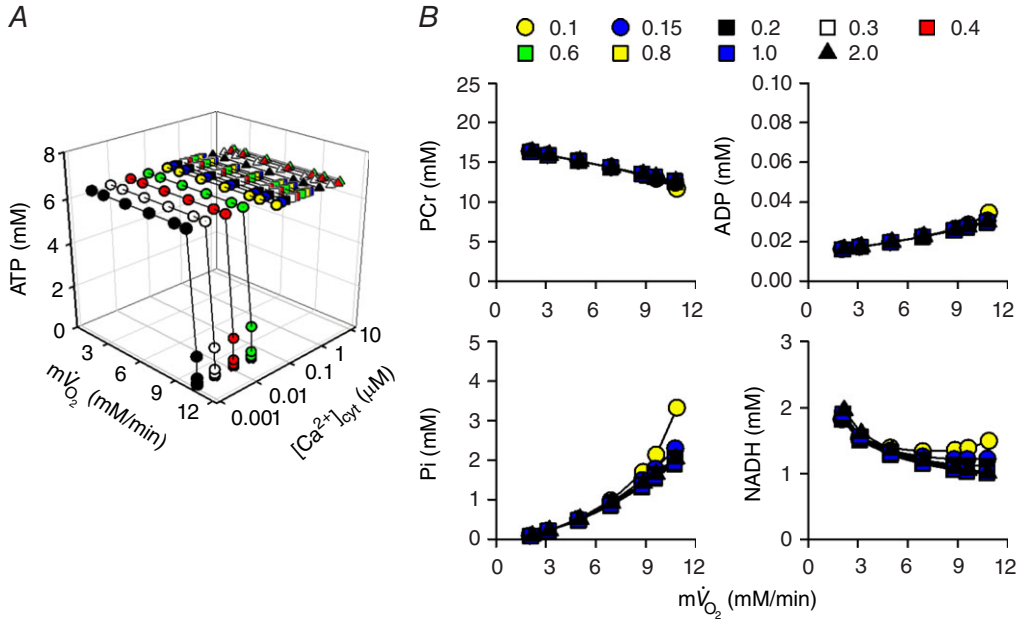

Figure 9. Workload and $[Ca^{2+}]_{cyt}$ dependences of energy metabolites in the simple cardiac cell model with multiple mitochondrial substrates: 1 mm malate, 5 mm glutamate, 0.3 mm pyruvate, 0.3 mm citrate, 0.1 mm 2-oxoglutarate and 3 mm aspartate
The same protocols as in Fig. 6 were used. *A*, total cytoplasmic ATP. *B*, cytoplasmic PCr, ADP, P_i and mitochondrial NADH.

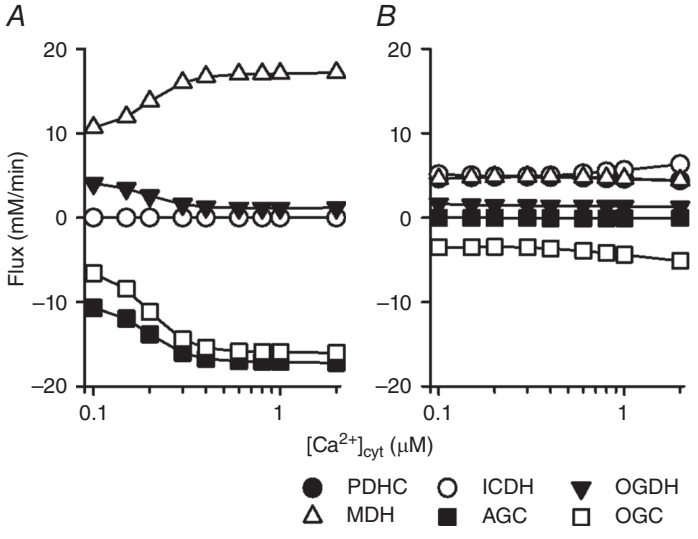

Figure 10. $[Ca^{2+}]_{cyt}$ dependence of four dehydrogenases, AGC and OGC
A, 5 mM malate and 5 mM glutamate condition. *B*, full substrates condition: 1 mM malate, 5 mM glutamate, 0.3 mM pyruvate, 0.3 mM citrate, 0.1 mM 2-oxoglutarate and 3 mM aspartate. $k_{ATPuse} = 1.5 \times 10^{-4}$ mM ms^{-1} ($m\dot{V}_{O_2} = 9.4$ – 9.8 mM min^{-1} in *A*, 8.8 – 8.9 mM min^{-1} in *B*).

influences on mitochondrial metabolism in the physiological range of $[Ca^{2+}]_{cyt}$.

The *in vitro* experiments referred to in this study used a high cytoplasmic Mg^{2+} (Territo *et al.* 2000; Bose *et al.* 2003; 5 mM), which attenuates Ca^{2+} influx through CaUni (Bragadin *et al.* 1979). Therefore, the Ca^{2+} influx may be larger under physiological conditions (approximately 1 mM Mg^{2+}) and $[Ca^{2+}]_{mit}$ may become higher than the present simulation condition. This possibility was tested in an additional simulation under a condition of increased CaUni activity to fit a $[Ca^{2+}]_{cyt}$–$[Ca^{2+}]_{mit}$ relation with 1 mM Mg^{2+} (Fig. S19*A*). Cytoplasmic ATP at high cardiac workload became stable even at lower $[Ca^{2+}]_{cyt}$ (0.03 μM; Fig. S19*B*) and the metabolites became further insensitive to $[Ca^{2+}]_{cyt}$ (Fig. S18*C*). These results further support our conclusion that Ca^{2+} has only a minor role in maintaining metabolite constancy under physiological conditions.

The $[Ca^{2+}]_{cyt}$-dependent activation of AGC had a significant influence on mitochondrial NADH level under the malate/glutamate condition. This result suggested that in addition to $[Ca^{2+}]_{mit}$, $[Ca^{2+}]_{cyt}$ also had a direct contribution to maintaining mitochondrial NADH level. This result is consistent with recent experiments in brain mitochondria, where the $[Ca^{2+}]_{cyt}$-dependent activation of AGC was found to be a key factor in adjusting mitochondrial energization to the requirements of neurons (Gellerich *et al.* 2012). However, the contribution of AGC to NADH may be dependent on mitochondrial substrates as shown in Fig. 10.

The stability of NADH and its Ca^{2+} dependence significantly depended on the substrate, especially on pyruvate. Several lines of experimental evidence are consistent with our finding. Wan *et al.* demonstrated that PDHC was almost 100% activated and NADH was insensitive to Ca^{2+} in the presence of pyruvate and malate, whereas PDHC was only 20% active in the absence of pyruvate and Ca^{2+}, and NADH level was activated by Ca^{2+} (2-oxoglutarate/malate condition) (Wan *et al.* 1989). Recently, Vinnakota *et al.* also reported that mitochondrial NADH level was almost insensitive to Ca^{2+} when pyruvate and malate were used as mitochondrial substrates (Vinnakota *et al.* 2011, 2016*b*). The present simulation study is in line with these results. However, since glutamate was omitted in Vinnakota *et al.*'s experiments, the contribution of AGC might have been underestimated. Minor roles of Ca^{2+} in mitochondrial metabolism are also consistent with data from mice lacking MCU, which showed normal or slightly reduced cardiac function (Holmstrom *et al.* 2015; Kwong *et al.* 2015; Wu *et al.* 2015).

P_i had pivotal roles in stimulating mitochondrial ATP production. In our model simulation, the allosteric activation of Complex III by P_i was a key factor in reproducing the experimental data (Figs 4 and 5). In the simple cardiac cell model, P_i increased with increasing

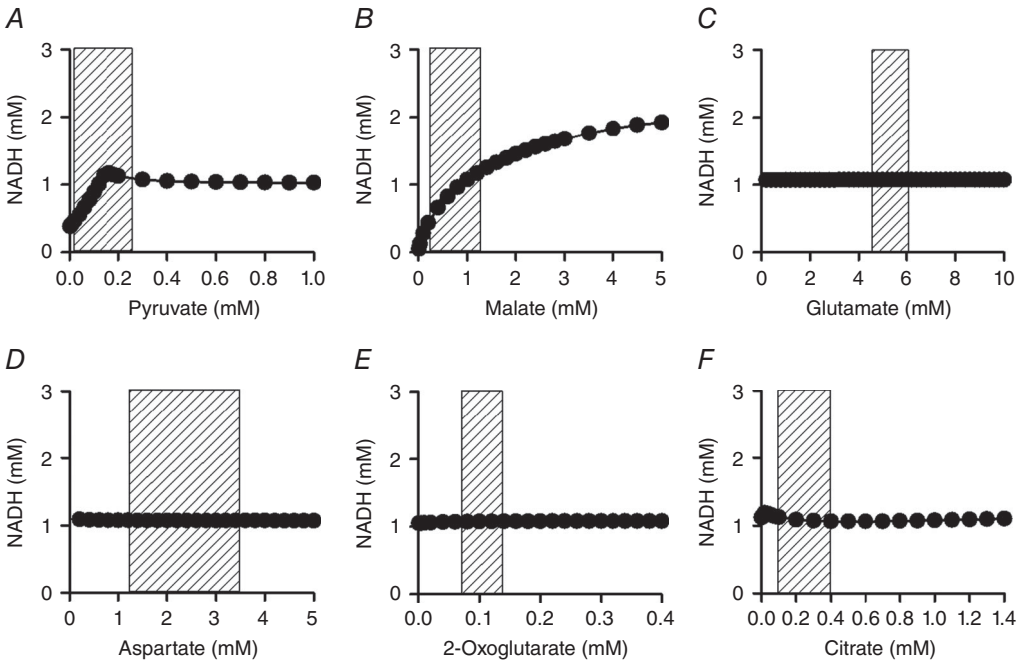

Figure 11. Substrate dependence of NADH in the simple cardiac cell model
The basic combination of substrates was the same as in Fig. 9. Pyruvate (*A*), malate (*B*), glutamate (*C*), aspartate (*D*), 2-oxoglutarate (*E*) and citrate (*F*) were systematically increased in the presence of 0.3 μM $[Ca^{2+}]_{cyt}$. k_{ATPuse} was set to 1.5×10^{-4} mM ms^{-1} ($m\dot{V}_{O_2}$ = 8.6–8.9 mM min^{-1}). Shaded areas show physiological range of each substrate (Albe *et al.* 1990; Kato *et al.* 2010).

workload (Figs 6 and 9), though the level was still within the physiological concentration range (3–5 mM) (Dos Santos *et al.* 2000; Shen *et al.* 2001). This tendency of P_i level was similar to the model simulation by Wu *et al.* (2008). Wu *et al.* (2008) also demonstrated the workload-dependent increase in P_i by analysing experimental data in the literature (Bache *et al.* 1999; Gong *et al.* 2003). The pooled data, however, had a large variation. On the other hand, Katz *et al.* (1989*a*) reported that P_i did not increase with increasing workload. Since detection of a low level of P_i is technically difficult, a new experimental technique is needed for more clearly detecting the increase of P_i during the cardiac workload transition. Most recently Vinnakota *et al.* (2016*a*) reported that P_i did not modulate the activity of Complex III in isolated mitochondria, in conflict with a previous report by Bose *et al.* (2013). Further studies are needed to determine whether or not P_i directly regulates Complex III.

Our cardiac mitochondrial model includes oxidative phosphorylation, substrate metabolism, and ion/substrate transporters. The main feature is that the major mitochondrial ion/substrate transporters and all the possible Ca^{2+}- and P_i-activated mechanisms are formulated so as to simulate mitochondrial ion dynamics, substrate metabolism and ATP production. To date, many mitochondrial models have been published, and some models can simulate additional mitochondrial functions such as reactive oxygen species formation (Yugi & Tomita, 2004; Korzeniewski *et al.* 2005; Cortassa *et al.* 2006; Jo *et al.* 2006; Zhou *et al.* 2006; Nguyen *et al.* 2007; Wu *et al.* 2007; Dzbek & Korzeniewski, 2008; Wu *et al.* 2008; Bazil *et al.* 2010; Wei *et al.* 2011; Kembro *et al.* 2013). However, to the best of our knowledge, this is the first simulation study to investigate the effects of mitochondrial substrate composition and Ca^{2+} on metabolite stability during workload transition. Many of the previous model studies did not extensively investigate the stability of metabolites during workload transition, and the regulatory effects of Ca^{2+} and P_i were not fully incorporated. Korzeniewski's group (Korzeniewski *et al.* 2005; Dzbek & Korzeniewski, 2008) studied metabolite stability, but their models did not include the citric acid cycle, metabolite transporters and mitochondrial Ca^{2+} dynamics. Wu *et al.* (2007, 2008) took a similar approach to ours in the study of metabolite stability and demonstrated that P_i was a primary feedback signal for stimulating oxidative phosphorylation. However, they did not consider the Ca^{2+}-dependent regulatory mechanisms, so that their model could not reproduce the experimental results of Territo *et al.* (2000).

The present simulation study has several limitations. Firstly, we based the model mainly on experimental data from isolated cardiac mitochondria, and the kinetics of enzymes and transporters in intact myocytes may be different from those in isolated mitochondria. Further improvement of the model will be required. However, in the present situation, it is practically impossible to obtain the kinetic parameters for mitochondrial enzymes and transporters *in vivo*. The simulation approach based on existing experimental data, as conducted in our present study, is the most promising way to understand mitochondrial function and energy metabolism *in vivo*. Secondly, glycolysis and β-oxidation of fatty acid were not incorporated in this model. We do not expect that the inclusion of glycolysis and β-oxidation would affect the main conclusion of this study because all of the components of the citric acid cycle, and PDHC, are activated by the substrates. However, it would be interesting to test in the future how flux balance between glycolysis and β-oxidation affects metabolite stability during workload transition. Lastly, although our model is based on existing experimental data, the mechanisms of some phenomena, such as Ca^{2+}-dependent activation of SN and P_i-dependent activation of Complex III, have not been well clarified. Further experimental studies to obtain the mechanistic insights are obviously needed to create a more realistic mathematical model.

References

Albe KR, Butler MH & Wright BE (1990). Cellular concentrations of enzymes and their substrates. *J Theor Biol* **143**, 163–195.

Allen DG & Kurihara S (1982). The effects of muscle length on intracellular calcium transients in mammalian cardiac muscle. *J Physiol* **327**, 79–94.

Andrienko T, Kuznetsov AV, Kaambre T, Usson Y, Orosco A, Appaix F, Tiivel T, Sikk P, Vendelin M, Margreiter R & Saks VA (2003). Metabolic consequences of functional complexes of mitochondria, myofibrils and sarcoplasmic reticulum in muscle cells. *J Exp Biol* **206**, 2059–2072.

Bache RJ, Zhang J, Murakami Y, Zhang Y, Cho YK, Merkle H, Gong G, From AH & Ugurbil K (1999). Myocardial oxygenation at high workstates in hearts with left ventricular hypertrophy. *Cardiovasc Res* **42**, 616–626.

Balaban RS (2009*a*). Domestication of the cardiac mitochondrion for energy conversion. *J Mol Cell Cardiol* **46**, 832–841.

Balaban RS (2009*b*). The role of Ca^{2+} signaling in the coordination of mitochondrial ATP production with cardiac work. *Biochim Biophys Acta* **1787**, 1334–1341.

Balaban RS, Kantor HL, Katz LA & Briggs RW (1986). Relation between work and phosphate metabolite in the in vivo paced mammalian heart. *Science* **232**, 1121–1123.

Bazil JN, Buzzard GT & Rundell AE (2010). Modeling mitochondrial bioenergetics with integrated volume dynamics. *PLoS Comput Biol* **6**, e1000632.

Beard DA (2006). Modeling of oxygen transport and cellular energetics explains observations on in vivo cardiac energy metabolism. *PLoS Comput Biol* **2**, e107.

Bernardi P (1999). Mitochondrial transport of cations: channels, exchangers, and permeability transition. *Physiol Rev* **79**, 1127–1155.

Boerth RC, Covell JW, Pool PE & Ross J Jr (1969). Increased myocardial oxygen consumption and contractile state associated with increased heart rate in dogs. *Circ Res* **24**, 725–734.

Bose S, French S, Evans FJ, Joubert F & Balaban RS (2003). Metabolic network control of oxidative phosphorylation: multiple roles of inorganic phosphate. *J Biol Chem* **278**, 39155–39165.

Bragadin M, Pozzan T & Azzone GF (1979). Kinetics of Ca^{2+} carrier in rat liver mitochondria. *Biochemistry* **18**, 5972–5978.

Brandes R & Bers DM (2002). Simultaneous measurements of mitochondrial NADH and Ca^{2+} during increased work in intact rat heart trabeculae. *Biophys J* **83**, 587–604.

Cha S & Parks RE Jr (1964). Succinic thiokinase. II. Kinetic studies: initial velocity, product inhibition, and effect of arsenate. *J Biol Chem* **239**, 1968–1977.

Chance B & Williams GR (1956). The respiratory chain and oxidative phosphorylation. *Adv Enzymol Relat Subj Biochem* **17**, 65–134.

Cortassa S, Aon MA, O'Rourke B, Jacques R, Tseng HJ, Marban E & Winslow RL (2006). A computational model integrating electrophysiology, contraction, and mitochondrial bioenergetics in the ventricular myocyte. *Biophys J* **91**, 1564–1589.

Dos Santos P, Aliev MK, Diolez P, Duclos F, Besse P, Bonoron-Adele S, Sikk P, Canioni P & Saks VA (2000). Metabolic control of contractile performance in isolated perfused rat heart. Analysis of experimental data by reaction:diffusion mathematical model. *J Mol Cell Cardiol* **32**, 1703–1734.

Dzbek J & Korzeniewski B (2008). Control over the contribution of the mitochondrial membrane potential ($\Delta\psi$) and proton gradient (ΔpH) to the protonmotive force (Δp). In silico studies. *J Biol Chem* **283**, 33232–33239.

Gellerich FN, Gizatullina Z, Trumbekaite S, Korzeniewski B, Gaynutdinov T, Seppet E, Vielhaber S, Heinze HJ & Striggow F (2012). Cytosolic Ca^{2+} regulates the energization of isolated brain mitochondria by formation of pyruvate through the malate-aspartate shuttle. *Biochem J* **443**, 747–755.

Glancy B & Balaban RS (2012). Role of mitochondrial Ca^{2+} in the regulation of cellular energetics. *Biochemistry* **51**, 2959–2973.

Gobel FL, Norstrom LA, Nelson RR, Jorgensen CR & Wang Y (1978). The rate-pressure product as an index of myocardial oxygen consumption during exercise in patients with angina pectoris. *Circulation* **57**, 549–556.

Gong G, Liu J, Liang P, Guo T, Hu Q, Ochiai K, Hou M, Ye Y, Wu X, Mansoor A, From AH, Ugurbil K, Bache RJ & Zhang J (2003). Oxidative capacity in failing hearts. *Am J Physiol Heart Circ Physiol* **285**, H541–H548.

Harris DA (1993). Regulation of the mitochondrial ATP synthase in rat heart. *Biochem Soc Trans* **21**, 778–781.

Hata K, Goto Y, Kawaguchi O, Takasago T, Saeki A, Nishioka T & Suga H (1994). Hypercapnic acidosis increases oxygen cost of contractility in the dog left ventricle. *Am J Physiol Heart Circ Physiol* **266**, H730–H740.

Holmstrom KM, Pan X, Liu JC, Menazza S, Liu J, Nguyen TT, Pan H, Parks RJ, Anderson S, Noguchi A, Springer D, Murphy E & Finkel T (2015). Assessment of cardiac function in mice lacking the mitochondrial calcium uniporter. *J Mol Cell Cardiol* **85**, 178–182.

Ingwall JS (2002). *ATP and the Heart*. Kluwer Academic Publishers, Dordrecht, Boston, London.

Jo H, Noma A & Matsuoka S (2006). Calcium-mediated coupling between mitochondrial substrate dehydrogenation and cardiac workload in single guinea-pig ventricular myocytes. *J Mol Cell Cardiol* **40**, 394–404.

Kato T, Niizuma S, Inuzuka Y, Kawashima T, Okuda J, Tamaki Y, Iwanaga Y, Narazaki M, Matsuda T, Soga T, Kita T, Kimura T & Shioi T (2010). Analysis of metabolic remodeling in compensated left ventricular hypertrophy and heart failure. *Circ Heart Fail* **3**, 420–430.

Katz A (2010). *Physiology of the Heart*. Lippincott Williams & Wilkins, Philadelphia.

Katz LA, Swain JA, Portman MA & Balaban RS (1989). Relation between phosphate metabolites and oxygen consumption of heart in vivo. *Am J Physiol Heart Circ Physiol* **256**, H265–H274.

Kembro JM, Aon MA, Winslow RL, O'Rourke B & Cortassa S (2013). Integrating mitochondrial energetics, redox and ROS metabolic networks: a two-compartment model. *Biophys J* **104**, 332–343.

Khouri EM, Gregg DE & Rayford CR (1965). Effect of exercise on cardiac output, left coronary flow and myocardial metabolism in the unanesthetized dog. *Circ Res* **17**, 427–437.

Kim B & Matsuoka S (2008). Cytoplasmic Na^+ dependent modulation of mitochondrial Ca^{2+} via electrogenic mitochondrial Na^+-Ca^{2+} exchange. *J Physiol* **586**, 1683–1697.

Kirichok Y, Krapivinsky G & Clapham DE (2004). The mitochondrial calcium uniporter is a highly selective ion channel. *Nature* **427**, 360–364.

Korzeniewski B (2007). Regulation of oxidative phosphorylation through parallel activation. *Biophys Chem* **129**, 93–110.

Korzeniewski B, Noma A & Matsuoka S (2005). Regulation of oxidative phosphorylation in intact mammalian heart in vivo. *Biophys Chem* **116**, 145–157.

Kwong JQ, Lu X, Correll RN, Schwanekamp JA, Vagnozzi RJ, Sargent MA, York AJ, Zhang J, Bers DM & Molkentin JD (2015). The mitochondrial calcium uniporter selectively matches metabolic output to acute contractile stress in the heart. *Cell Rep* **12**, 15–22.

McCormack JG, Halestrap AP & Denton RM (1990). Role of calcium ions in regulation of mammalian intramitochondrial metabolism. *Physiol Rev* **70**, 391–425.

Murphy E, Coll KE, Viale RO, Tischler ME & Williamson JR (1979). Kinetics and regulation of the glutamate-aspartate translocator in rat liver mitochondria. *J Biol Chem* **254**, 8369–8376.

Nguyen MH, Dudycha SJ & Jafri MS (2007). Effect of Ca^{2+} on cardiac mitochondrial energy production is modulated by Na^+ and H^+ dynamics. *Am J Physiol Cell Physiol* **292**, C2004–C2020.

Pardo B, Contreras L, Serrano A, Ramos M, Kobayashi K, Iijima M, Saheki T & Satrustegui J (2006). Essential role of aralar in the transduction of small Ca^{2+} signals to neuronal mitochondria. *J Biol Chem* **281**, 1039–1047.

Rodriguez-Zavala JS, Pardo JP & Moreno-Sanchez R (2000). Modulation of 2-oxoglutarate dehydrogenase complex by inorganic phosphate, Mg^{2+}, and other effectors. *Arch Biochem Biophys* **379**, 78–84.

Saks V, Kuznetsov AV, Gonzalez-Granillo M, Tepp K, Timohhina N, Karu-Varikmaa M, Kaambre T, Dos Santos P, Boucher F & Guzun R (2012). Intracellular Energetic Units regulate metabolism in cardiac cells. *J Mol Cell Cardiol* **52**, 419–436.

Sarai N, Matsuoka S & Noma A (2006). simBio: a Java package for the development of detailed cell models. *Prog Biophys Mol Biol* **90**, 360–377.

Satrustegui J, Pardo B & Del Arco A (2007). Mitochondrial transporters as novel targets for intracellular calcium signaling. *Physiol Rev* **87**, 29–67.

Shen W, Tian R, Saupe KW, Spindler M & Ingwall JS (2001). Endogenous nitric oxide enhances coupling between O_2 consumption and ATP synthesis in guinea pig hearts. *Am J Physiol Heart Circ Physiol* **281**, H838–H846.

Shimizu J, Todaka K & Burkhoff D (2002). Load dependence of ventricular performance explained by model of calcium-myofilament interactions. *Am J Physiol Heart Circ Physiol* **282**, H1081–H1091.

Takeuchi A, Kim B & Matsuoka S (2015). The destiny of Ca^{2+} released by mitochondria. *J Physiol Sci* **65**, 11–24.

Territo PR, French SA, Dunleavy MC, Evans FJ & Balaban RS (2001). Calcium activation of heart mitochondrial oxidative phosphorylation: rapid kinetics of mVO_2, NADH, AND light scattering. *J Biol Chem* **276**, 2586–2599.

Territo PR, Mootha VK, French SA & Balaban RS (2000). Ca^{2+} activation of heart mitochondrial oxidative phosphorylation: role of the F_0/F_1-ATPase. *Am J Physiol Cell Physiol* **278**, C423–C435.

Vinnakota KC, Bazil JN, Van den Bergh F, Wiseman RW, Beard DA (2016a). Feedback regulation and time hierarchy of oxidative phosphorylation in cardiac mitochondria. *Biophys J* **23**, 972–980.

Vinnakota KC, Dash RK & Beard DA (2011). Stimulatory effects of calcium on respiration and NAD(P)H synthesis in intact rat heart mitochondria utilizing physiological substrates cannot explain respiratory control in vivo. *J Biol Chem* **286**, 30816–30822.

Vinnakota KC, Singhal A, Van den Bergh F, Bagher-Oskouei M, Wiseman RW & Beard DA (2016b). Open-loop control of oxidative phosphorylation in skeletal and cardiac muscle mitochondria by Ca^{2+}. *Biophys J* **110**, 954–961.

Wan B, LaNoue KF, Cheung JY & Scaduto RC Jr (1989). Regulation of citric acid cycle by calcium. *J Biol Chem* **264**, 13430–13439.

Wei AC, Aon MA, O'Rourke B, Winslow RL & Cortassa S (2011). Mitochondrial energetics, pH regulation, and ion dynamics: a computational-experimental approach. *Biophys J* **100**, 2894–2903.

Wu F, Yang F, Vinnakota KC & Beard DA (2007). Computer modeling of mitochondrial tricarboxylic acid cycle, oxidative phosphorylation, metabolite transport, and electrophysiology. *J Biol Chem* **282**, 24525–24537.

Wu F, Zhang EY, Zhang J, Bache RJ & Beard DA (2008). Phosphate metabolite concentrations and ATP hydrolysis potential in normal and ischaemic hearts. *J Physiol* **586**, 4193–4208.

Wu F, Zhang J & Beard DA (2009). Experimentally observed phenomena on cardiac energetics in heart failure emerge from simulations of cardiac metabolism. *Proc Natl Acad Sci U S A* **106**, 7143–7148.

Wu Y, Rasmussen TP, Koval OM, Joiner ML, Hall DD, Chen B, Luczak ED, Wang Q, Rokita AG, Wehrens XH, Song LS & Anderson ME (2015). The mitochondrial uniporter controls fight or flight heart rate increases. *Nat Commun* **6**, 6081.

Yugi K & Tomita M (2004). A general computational model of mitochondrial metabolism in a whole organelle scale. *Bioinformatics* **20**, 1795–1796.

Zhou L, Cabrera ME, Okere IC, Sharma N & Stanley WC (2006). Regulation of myocardial substrate metabolism during increased energy expenditure: insights from computational studies. *Am J Physiol Heart Circ Physiol* **291**, H1036–H1046.

Additional information

Competing interests

The authors declare that they have no conflicts of interest with the contents of this article.

Author contributions

All studies were performed at Kyoto University, Ritsumeikan University and University of Fukui. R.S. created most of models of enzymes and transporters. A.T. created a simple cardiac cell model implemented with mitochondria, analysed the model and wrote the paper. Y.H. created models of ion transporters. N.I. conceived the idea for the project. S.M. conceived the idea for the project, analysed the model, and wrote the paper with A.T. All authors approved the final version of the manuscript and agree to be accountable for all aspects of the work in ensuring that questions related to the accuracy or integrity of any part of the work are appropriately investigated and resolved. All persons designated as authors qualify for authorship, and all those who qualify for authorship are listed.

Funding

This work was supported by the leading project for Biosimulation (A.T., N.I. and S.M.), the Biomedical Cluster Kansai project (Y.H., N.I. and S.M.), and JSPS KAKENHI grant Numbers 26670101 (S.M.), 15H04674 (S.M.), and 26291019 (A.T.).

Acknowledgements

We are grateful to Dr Akinori Noma for his valuable suggestions and support.

Supporting information

The following supporting information has available in the online version of this article.

Appendix. Model variables, parameters and equations.
Source Code S1. Source codes of components written in Java class.
XML S1. An XML file to execute simulations of isolated mitochondrial experiments by Bose *et al.* (2003).
XML S2. An XML file to execute simulations of isolated mitochondrial experiments by Territo *et al.* (2000).
XML S3. An XML file to execute simulations using a simple cardiac cell model with full substrates.
XML S4. An XML file to execute simulations using a simple cardiac cell model with malate/glutamate.
Figure S1. Kinetic studies of the reaction catalysed by CS.
Figure S2. Kinetic studies of the reaction catalysed by ACO.
Figure S3. Kinetic studies of the reaction catalysed by ICDH.
Figure S4. Kinetic studies of the reaction catalysed by OGDH.
Figure S5. Kinetic studies of the reaction catalysed by SCS.
Figure S6. Kinetic studies of the reaction catalysed by SDH.
Figure S7. Kinetic studies of the reaction catalysed by FH.
Figure S8. Kinetic studies of the reaction catalysed by MDH.
Figure S9. Kinetic studies of the reaction catalysed by NDK.
Figure S10. Kinetic studies of the reaction catalysed by AST.
Figure S11. Kinetic studies of the reaction catalysed by PDHC.
Figure S12. Kinetic studies of the reaction catalysed by PC.
Figure S13. Kinetic studies of the reaction catalysed by ALT.
Figure S14. Time courses of NADH and $\Delta\Psi$ changes in the simulation of experiment by Bose *et al.* (2003).
Figure S15. $[Ca^{2+}]_{cyt}$ dependence of mitochondrial model.
Figure S16. Ca^{2+} dependences of enzymes and transporters.
Figure S17. $[P_i]_{mit}$ dependences of OGDH, SCS and C3.
Figure S18. Workload and $[Ca^{2+}]_{cyt}$ dependences of energy metabolites in the simple cardiac cell model without metabolite controls.
Figure S19. Workload and $[Ca^{2+}]_{cyt}$ dependences of energy metabolites in the simple cardiac cell model with increased activity of CaUni.